ESA Contract No. 4000115171/15/F/MOS

Benchmarking re-entry prediction uncertainties

Executive Summary

Team:
TU Delft, The Netherlands
HTG, Germany
BAS, United Kingdom

14 March 2017

1 Introduction

The primary objective of the *Benchmarking re-entry prediction uncertainties* study is to fully exploit the information content of the GOCE observations and telemetry collected during its reentry phase for better understanding re-entry predictions in general and for GOCE in particular (ESA, 2015). Down to an altitude of 137 km, a rich data set of high-quality GPS, star tracker and also accelerometer observations were collected, be it that the latter were more and more saturated.

In order to meet the study objective the following tasks were defined:

1. High accuracy orbit determination (WP110, 120 & 130):

   The unique GOCE observational data sets allows to compute high-precision orbits. In addition, high-precision non-gravitational accelerations can be estimated for validating and augmenting (in case of saturations) the accelerometer observations, and althus provide information about the GOCE drag environment down to 130 km altitude;

2. Re-entry prediction uncertainties (WP210 & 220):

   Based on the high-precision GPS-based GOCE orbit solution, uncertainties associated with reentry predictions during a satellite's final phases (GOCE in particular) can be studied. Uncertainties are not only due to errors in non-gravitational, predominantly drag, models, but also due to sparse tracking during final reentry phases (e.g. TIRA-based);

3. Rigid-body re-entry predictions (WP310 & 320):

   GOCE's aerodynamic shape is to a certain degree similar to a class of used rocket bodies and payloads. It is therefore interesting to investigate to which degree the results on the uncertainties derived for the GOCE re-entry can be applied to rigid bodies of similar aerodynamic characteristics.

4. Critical assessment (WP410):

   The outcome of Tasks 1-3 will be critically assessed to arrive at conclusions and recommendations.

2 High accuracy orbit determination

2.1 Precise orbits (WP110)

Reduced-dynamic orbit solutions were produced for the final phase of the GOCE mission, covering a period from 19 October to 10 November 2013 (i.e. two days before the ion engines ran out of fuel). Starting October 21, the orbital altitude decayed from around 250 km to 137 km and the atmospheric drag increased exponentially from about 10,000 nm/s^2 on 21 October 2013 to over 300,000 nm/s^2 after 12:00 hr on 10 November 2013. It was shown that the extended Kalman filter implemented in the DLR GHOST software is capable of estimating such high non-gravitational acceleration levels and is capable of providing orbit solutions that are consistent to below the dm level in terms of 2-hr orbital arc overlaps and with independent SLR observations. Moreover, the orbits fit the ionospheric-free GPS carrier-phase observations down to levels of a few cm as well. The consistency with the GOCE HPF reduced-dynamic PSO solutions is at the few dm level or better, except for the last couple of days. However, for these last two days the consistency with the GOCE HPF PSO kinematic orbit solutions is still below a few dm, except for a few outliers. The latter indicates the high quality of the GHOST extended Kalman filter orbit solutions until the end of the high-quality GPS data availability.

The non-gravitational accelerations that were estimated by the extended Kalman filter compare very well with the common-mode accelerometer observations, as long as the accelerometers are not saturated. This is especially true for the X axis, which is closely aligned with the flight or along-track direction. High correlations were found between the estimated non-gravitational accelerations and those from the accelerometers during all periods when they were not saturated: typically close to 0.99 for the X axis of the gradiometer reference frame, for which the non-gravitational acceleration signal is by far the largest. Also high correlations were found for the other two axes: between 0.63 and 0.99 for the Y axis (close to the cross-track direction), and up to 0.93 for the Z axis (close to the height direction). The highest correlations were found for the last days, as long as the accelerometers were not saturated. It might be claimed that the GPS-based estimated accelerations provide valuable information about the non-gravitational accelerations for periods when the accelerometers were saturated, especially close to the end of the GPS high-quality data availability down to an altitude of 137 km.

An example showing the high level of consistency between accelerometer observed and GPS-based non-gravitational accelerations is displayed in Figure 1.

2.2 Numerical atmosphere modeling (WP120)

A series of simulations with the Whole Atmosphere Community Climate Model eXtension (WACCM-X) was carried out to model the atmospheric state along the GOCE trajectory and test the influence of different drivers of atmospheric variability. WACCM-X is a global chemistry-climate model that extends from the surface up to about 500 km altitude. A full description of WACCM-X is given by Liu et al. (2010) and references therein. Table 1 provides an overview of the simulations performed with the model (see Chapter 3 of the Final Report for details (TU DELFT et al., 2017)).

2.3 Acceleration analysis (WP130)

The thermosphere densities along the GOCE trajectory from the WP120 WACCM-X model simulations were analysed, along with densities computed using various other empirical and physics-based first-principles models. The density data could be compared with observations derived from the gradiometer DFACS channel data, as well as those derived from the GPS-derived acceleration data. In general, the DFACS and GPS-derived accelerations and densities were in excellent agreement, with the DFACS data showing slightly more high-frequency signal variability, but lower coverage during the final days due to accelerometer saturation.

The analysis of the various WACCM-X runs resulted in the conclusion that solar and geomagnetic activity variability were the major drivers behind changes in atmospheric drag on the GOCE orbit. The modified lower boundary condition also had a large impact on densities, but only at time and spatial scales of the order of a fraction of the orbit. The effect therefore tended to average out in the drag effect on the orbit. The lunar tide and solar proton event cases showed only negligible differences with the control case, indicating that these drivers do not need to be further investigated with high priority.

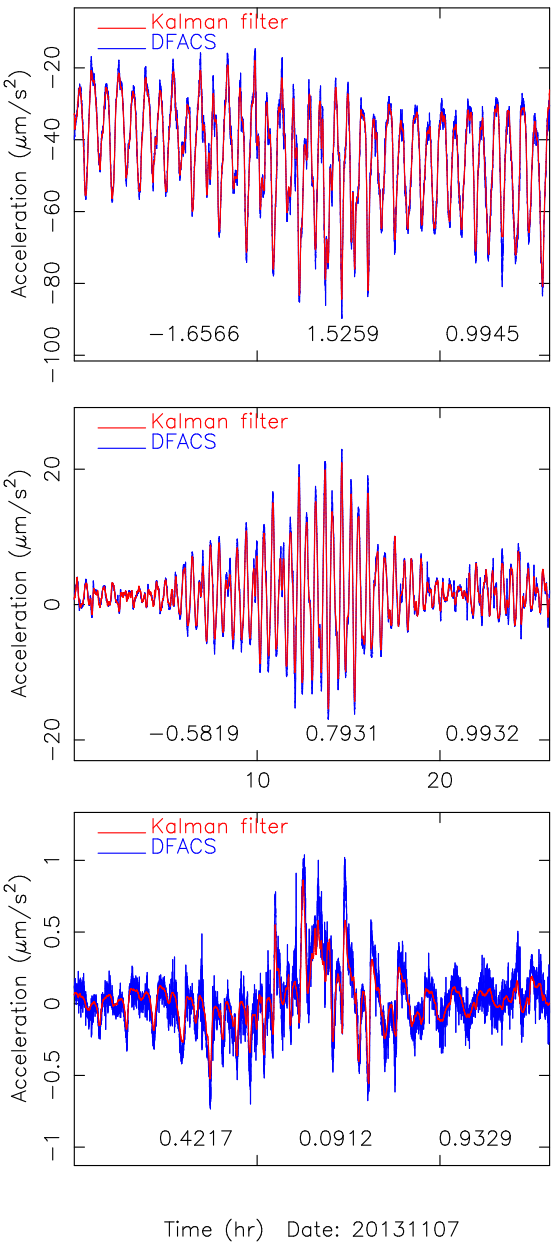

Figure 1: Estimated empirical accelerations compared to GOCE observed common-mode accelerations, both in the GRF, for 7 November 2013 (X, Y, Z axis from top to bottom)

Ident.	Description	Solar radiation	Geomagnetic activity	SPE	Lower boundary	Lunar tide
control	Control	As observed	As observed	As observed	Nudged to observations	On
freelb	Free-running lower boundary	As observed	As observed	As observed	Free running	On
nolunt	No lunar tide	As observed	As observed	As observed	Nudged to observations	Off
fixrad	Fixed solar radiation	Constant average value	As observed	As observed	Nudged to observations	On
fixmag	Fixed geomagnetic activity	As observed	Constant average value	As observed	Nudged to observations	On
fixspe	Fixed SPE ion pair production	As observed	As observed	Constant average value	Nudged to observations	On

Table 1: Overview of the simulations performed with WACCM-X.

The data and models were compared in a variety of ways. As an example, the orbit-averaged GPS-observed over model density ratio time series for several models is summarized in Figure 2.

The Figure shows that all models produce densities that are lower than the observations, since all ratios are lower than 1.0. This can be partly due to the use of the ESA-supplied 44-panel geometry model of the satellite (originating at Alenia), which results in a roughly 20% too large ballistic coefficient, compared to HTG's ANGARA model of GOCE. But even after correcting for this, the average modeled densities for all models were still larger than the observations during this timeframe. On top of this, our analysis showed that the solar flux predictions used at ESOC resulted in even larger predicted densities. These factors combined would have contributed to an earlier than realistic predicted re-entry time, in the weeks leading up to the event.

Returning to the model comparison, as expected, the HASDM model has by far the best performance. This model is the only one for which data (from classified US space surveillance tracking) on the orbital decay of other satellites and space debris (so-called calibration objects) are used to adjust to the real state of the thermosphere. After November 7, the time series for HASDM ratios starts to deviate upwards from its long-term average of 0.7, indicating that the relative overprediction of the model is reduced at lower altitudes. This change in trend could be caused by an underrepresentation of calibration object with such low perigees.

The WACCM-X model is by far the most complex of these models, incorporating the physics and chemistry of the entire atmosphere. It also shows the worst performance, indicating that this complexity is not yet fully mastered, and does not yet lead to a higher accuracy than more simple empirical models. The value of models such as WACCM-X is in science, not in operations.

Both the JB-2008 and DTM-2013 models outperform the NRLMSISE-00 model, which for many years has been the de-facto standard thermosphere model. It should be noted, however, that the input file with proxies for JB-2008 have received various updates in the past years, containing adjustments to the calibration of the space-based observations of solar irradiance. The model developers have therefore been able to adjust this calibration to improve the thermospheric model performance, giving them perhaps an unfair advantage over the NRLMSISE-00 and DTM-2013 models, which use ground-based solar radio flux observations instead, which do not have these calibration issues. The JB-2008 model, with these updated proxies, can perhaps be seen as an intermediate model between the traditional semi-empirical density models, and the fully calibrated HASDM model.

The differences between the models that can be observed in this plot cannot be pinpointed to a single source. They originate from a combination of the different data sets used to generate the models, the parametric equations that define the models, and of course the different sets of proxies and indices.

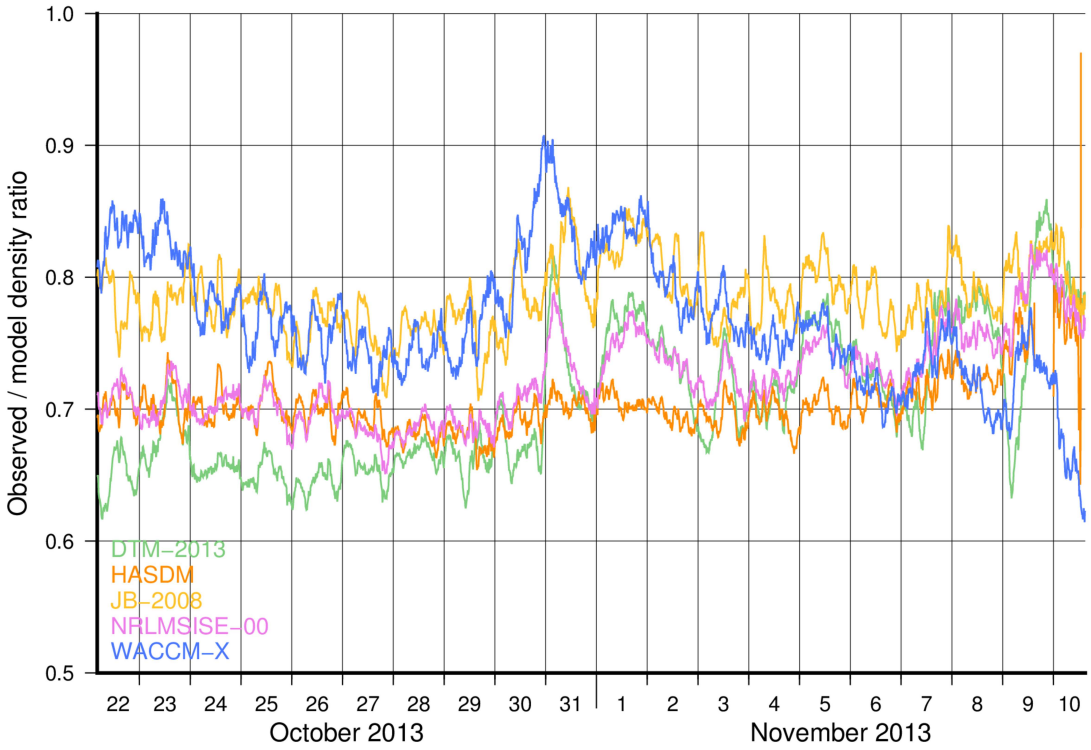

Figure 2: Orbit-average observed / modeled density ratio time series during the GOCE deorbit phase, comparing 5 models with GOCE GPS-derived density data.

3 Re-entry prediction uncertainties

3.1 GOCE re-entry observations (WP210)

TIRA tracking observations of GOCE during the final stages of its mission were analyzed and used for GOCE orbit determination. In addition, an analysis of real GOCE Two-Line Elements (TLE) data was conducted plus the simulation of such data. The TIRA-based orbit solutions confirm the results by Lemmens et al. (2015), showing that TIRA-based orbit solutions typically have position errors of the order of a few kms up to more than 15 km for GOCE (Figure 3).

It was found that enhancements made to TLEs have resulted in a reduced initial uncertainty and improved (forward) propagation stability. However, it is important to be aware of differences, such as the reduced backward propagation accuracy and difference in ballistic coefficient. Especially, as both types can occur in the same period. Therefore, it is not recommended to mix both types in analyses. Fortunately, it is straightforward to distinguish between both types. As a result of this, two TLE input sets for re-entry simulations were considered, namely enhanced and classic initial state and uncertainty.

The estimation of an initial covariance matrix for re-entry simulations gave mixed results. The initial uncertainty and strong correlations can be estimated reliably, while (weak to moderate) correlations proved to be more difficult. This is partly due to sensitivity of the correlations.

The simulated TLEs, using perfect observations and an idealised observation scenario, illustrated the limitations of the SGP4 model and how close actual TLEs (especially eTLEs) approach this. The addition of noise replicated uncertainties in the observations. Accurate solutions were affected more, resulting in overall less accuracy, but more consistency. Noise was found to have a negligible effect on the estimation of $\beta^\star$ (related to the ballistic coefficient).

By simulating TLEs their expected accuracy can be analysed for various orbital and space weather scenarios. Moreover, by comparing actual TLEs against simulated TLEs, the performance of the SSN can be assessed. To improve the fidelity of simulated TLEs, further research should focus on improving the stability of the

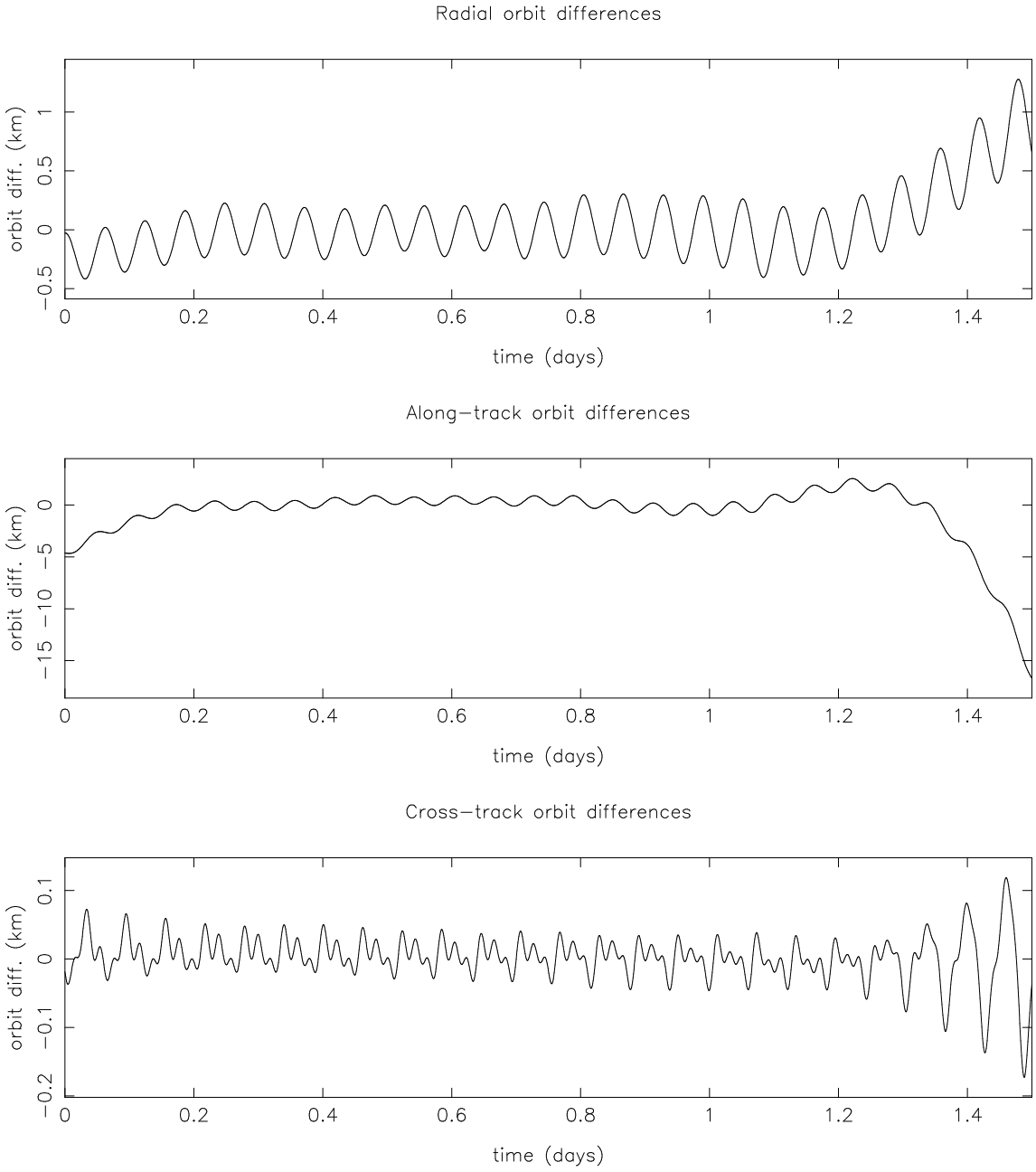

Figure 3: Orbit differences between GHOST Kalman filter and GEODYN TIRA-based orbit solutions for 131109 00:00 - 131110 12:00

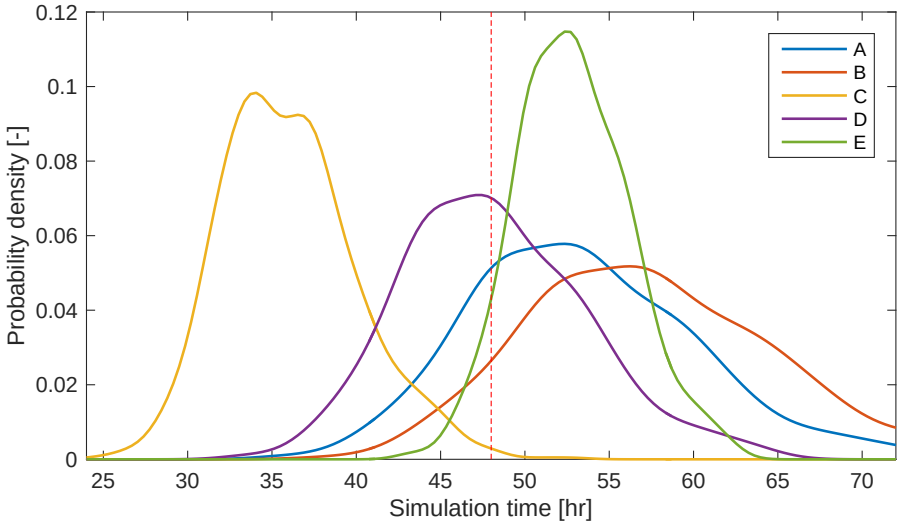

Figure 4: Decay-time distributions for different modelling scenarios, compared to the true re-entry epoch (indicated by the dashed red line).

determination process and on implementing a determination process akin to enhanced TLEs. Specifically, the sensitivity to the observation span should be addressed first, which was now determined through trial and error.

3.2 GOCE re-entry predictions (WP220)

Statistical re-entry predictions

Re-entry predictions of decaying objects can help determine (and exclude) possible impact locations. Due to uncertainties in the initial state and models, the impact location and time are also stochastic variables. The spread of possible impact locations is generally concentrated along the orbital ground track. Moreover, at about 80 km altitude the exponentially increasing atmosphere causes objects to break up, followed by impact mere minutes later. Thus instead of the true impact epoch and location, decay epoch and location are considered. In this study re-entry predictions, in the form of decay-time distributions, are obtained by propagating the initial uncertainty using a Monte-Carlo (MC) re-entry simulator.

Both the translational (position and velocity) and rotational (attitude and rotational rates) are modelled. The aerodynamic interaction (forces and moments) of GOCE are modelled as a rigid body. Moreover, three separate flow regimes are considered, namely the free-molecular, transitional and continuum flow regimes, to account for the substantial change in atmospheric properties along the re-entry trajectory.

GOCE was equipped with magnetorquers to stabilise its attitude. These torquers continued to function throughout the re-entry. A simple linear-quadratic regulator is implemented to simulate the attitude control.

The effect of the different modelling efforts is shows in Figure 4 with respect to the best realistic prediction scenario (A: GPS-derived uncertainties with full modelling). Idealised (B) and no control (C) scenarios are investigated. Also the an unbiased (D) and less uncertain (E) atmospheric models are investigated. Figure 5 shows the result of different input sources, namely TIRA (F), simulated TIRA (G), enhanced TLEs (H), and classic TLEs (I).

Case B is representative of traditional 3DOF predictions. It overshoots the true decay time by almost 10 hours, not accounting for small variations in the aerodynamic angles and tumbling after controller saturation are not accounted for. Case C, on the other hand, neglects completely neglects the control, resulting a gross underestimation of the decay time. Due the aerodynamic shape of GOCE, the drag coefficient of a stable attitude is nearly 3 times lower than for tumbling motion.

The density during the re-entry of GOCE was significantly lower than predicted. By not accounting for the re-entry times are again underestimated as illustrated by Case D. Finally, the re-entry prediction uncertainty is reduced by almost 40% if the atmospheric uncertainty is halved.

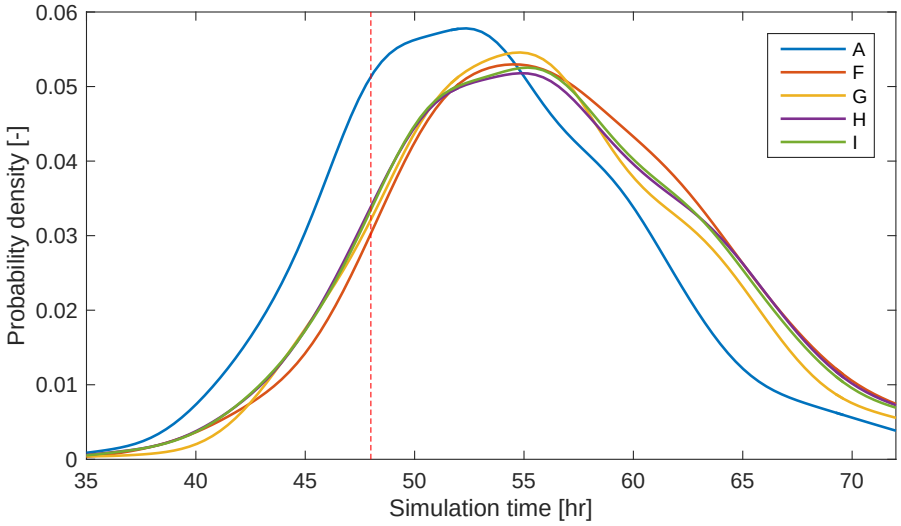

Figure 5: Decay-time distributions for different input states.

The effects of using different sources for the initial state, initial state uncertainty, and atmospheric uncertainty bias is observed by comparing Cases F to I with A (GPS). Cases F to I are very interesting, as they present non-cooperative methods of determining an objects state. In all cases the decay-time distributions are wider, which is to be expected due to increased uncertainty in the initial state. The differences between amongst Cases F to I are even less.

The differences of the different sources is surprisingly small, considering that the positional accuracy is in the order of decimetres for GPS and kilometres for TIRA. This illustrates the moderate significance of positional uncertainty on the final decay-time distributions.

The decay-time distribution accuracy is dominated primarily by the attitude control and the atmospheric bias. The attitude control can prolong the re-entry significantly. For a TTD of 2 days, the median was demonstrated to lie anywhere between 17 and 55 hours depending on till when the controller was able to maintain a stable attitude. Moreover, the control negates most influence of the initial rotational uncertainty.

It is important to properly account for attitude control and should receive attention for cases where a satellite remains actively or passively controlled during re-entry.

The decay-time distribution precision is dominated by the atmospheric uncertainty, outweighing all other contributions in the uncertainty modelling effort. This is especially clear from the width of the distributions obtained from the different state sets. The prediction ability is only improved marginally, by knowing the translational state at decimetre (GPS) compared to kilometre level (TLE). This is further demonstrated that halving the atmospheric uncertainty, nearly halves the decay-time uncertainty.

Parametric models for re-entry predictions

Several parametric and non-parametric distributions are fit to the decay-time distributions and assessed using the one-sample Kolmogorov-Smirnov test. Table 2 shows the test value (maximum distance between sample and modelled cumulative density function; lower is better) for each object and starting epoch. The first entry is GOCE, the next five entries are the three Delta-K rocket body, the last entry is CHAMP.

Figure 6 shows the result of the fitting process for GOCE. A histogram of the dataset with on hour bins is shown, as well as the original KDE for GOCE.

The non-parametric kernel-density estimate, provides the best fit in a variety of situation. Parametric distributions, use a few parameters to represent a distributions. The parametric distributions are therefore unable to completely represent (complex) features in the distributions. Per orbit features naturally become more pronounced as the time till decay (TTD) is shorter. Regarding the parametric distributions, the normal distribution performs unsatisfactory in almost all cases, while skew normal performs best, (closely) followed by the log normal. The skew normal has one extra parameter (3 in total), giving the distribution more degrees of freedom. No closed-form solution exists for the parameters, so they can only be computed numerically. A trade-off between complexity and performance should be made depending on the application. Specialised distributions

Object	TTD [hr]	KDE	Normal	Log-N	Gumbel	Gamma	Skew-N
34602	48	0.023	0.043	0.021	0.039	0.026	0.018
28130	6.3	0.035	0.082	0.064	0.056	0.071	0.046
28486	26	0.030	0.055	0.069	0.140	0.058	0.047
28486	8.7	0.025	0.060	0.042	0.057	0.046	0.043
33592	27	0.026	0.057	0.039	0.040	0.042	0.030
33592	3.1	0.030	0.150	0.118	0.065	0.129	0.121
26405	48	0.017	0.067	0.035	0.030	0.046	0.034

Table 2: One-sample KS-test statistic of different statistical distributions for several objects and different time to decay (TTD).

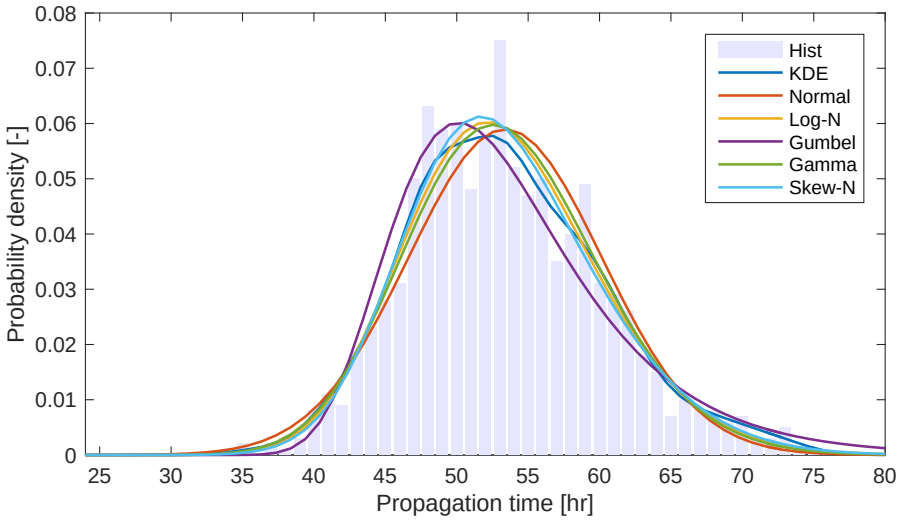

Figure 6: Decay-time distributions and several (non)parametric fits.

like Gumbel can work out very well in specific cases, but lack general applicability.

4 Rigid-body re-entry predictions

4.1 Rigid body dynamics (WP310)

One of the aims of this study was to find analogies between the re-entry of GOCE and other spacecraft of comparable attitude behaviour by comparing the aerodynamic coefficients. As a baseline approach solutions for the aerodynamic coefficients of simple-shaped bodies in free-molecular flow were derived. The approach used differs from previous approaches in the use of a more symbolic notation, which made it possible to find more compact expressions for the coefficients, and a different consideration of normal and tangential components.

The advantage of a more manageable form of the coefficients was the possible application to real satellites. This was done for the GOCE satellite, where with a simple surrogate box model the coefficients of the full model calculated by a Monte-Carlo method could be quite accurately reproduced by an analytical calculation. For a simplified geometric ATV model the analytical approach led also to reasonable results compared to Monte Carlo calculations.

The analytical approach was furthermore applied to a rocket body (Delta rocket body) and another LEO satellite (CHAMP). While the shape of rocket bodies can be quite accurately described by simple ge- ometric models, resulting in very good agreement between numerical and analytical calculations, the application to more complex shapes (varying cross-sections) is more challenging. While still reason- able approximations can be found, additional dedicated analytical formulas for certain classes of shapes should be derived for a more quantitative approximation. For a principal understanding of the trajectory and attitude motion less strict agreement is necessary than for long-term predictions.

4.2 Re-entry prediction accuracy validation (WP320)

It is investigated how well previous findings translate to other more generic bodies. However, GOCE was a very unique satellite. Especially due to the ion-thruster, strong attitude control, and aerodynamic design. The ion thruster was switched off on October 21, 2013, so are not accounted for in the re-entry predictions. The attitude controller, however, makes it hard to hard to compare to other satellites and bodies. The slender shape of GOCE is akin to rocket stages.

As test objects CHAMP and three Delta-K rocket bodies are selected. For the Delta-Ks multiple re-entries, aerodynamic models, and results from previous studies are available. The initial uncertainty is estimated using the same method as for GOCE.

For the Delta-Ks the initial uncertainty varies significantly per object. The initial translational accuracy of the Delta-Ks varies between 40% and 95% of GOCE's estimated accuracy, despite the the high interest in GOCE and stable attitude. The slightly better accuracy can be explained by the eccentric orbits of the Delta-Ks, improving their TLE accuracy. The uncertainty of CHAMP is also slightly larger than the Delta-K rocket stages and comparable to GOCEs.

Overall, it can be seen that the uncertainty, correlations, and error growth differ a lot amongst the different objects. This further illustrates that using a single error model is not representative, even if the objects are very similar.

Rigid body re-entry simulations are troubled by the large unknowns in the initial rotational state. Analysis of 34 Delta-K rocket bodies shows that there is a lot of variation in ballistic coefficients: amongst the rocket bodies (ranging between 60 and over 200 $\mathrm{kg\,m^{-2}}$) and over the two week prior to re-entry for a single body.

Possible sources for these variations in the retrofit ballistic coefficients include: differences in mass, errors in density modelling, errors in state estimation, differences in rotational state. Given the multiplicity of possible sources, it remains difficult at this stage to draw any conclusions on differences in rotational state and/or atmospheric density errors amongst these objects. Therefore, no improvement to uncertainty model of the initial rotational state could be made.

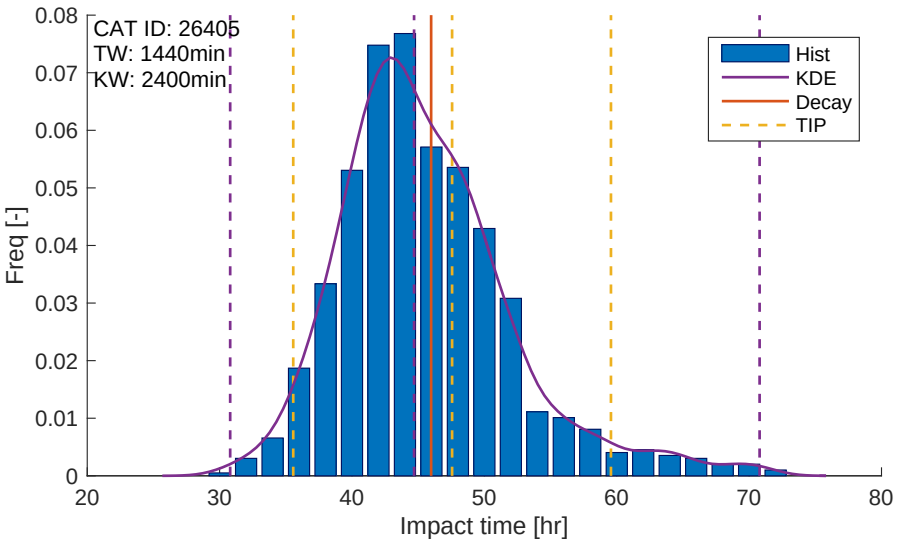

Figure 7: Decay-time distribution of CHAMP, compared with true decay epoch and TIP.

For CHAMP, the retrofit ballistic coefficient starts to increase after September 5, 2010 indicating a transition from a stable to tumbling attitude. By assuming a tumbling state, the ratio of modelled and observed atmospheric density could be estimated, which is used to bias the density for the re-entry predictions.

Re-entry predictions are obtained for the three Delta-Ks and CHAMP. Compared to previous studies the initial uncertainty estimation (per object instead of fixed from literature) and atmospheric uncertainty model (log-normal instead of uniform) are improved. The resulting distributions are wider than previous, as the tails of log-normal distribution fall outside the uniform bounds, resulting in samples with shortened and prolonged decay-times. This finding is in line with previous studies, which suggested an under-representation of the extremes of the obtained distributions. However, given the limited sample size and large uncertainty in the atmosphere and rotational state, it is difficult to validate improvements to re-entry simulation models.

Further investigation should include all original Delta-K cases, additional (more recent) Delta-Ks, and other large groups of (rocket) bodies, to increase the sample size and statistical validity.

Figure 7 shows the results of the re-entry simulation of CHAMP performed 48 hours before the true decay epoch.

The 99.73% width of the re-entry simulation is 66% wider than the TIP window (unknown confidence). The median of the re-entry simulations and TIP are relatively close to the true decay epoch. The increased width is attributed to the uncertainty in the density and rotational state. To improve re-entry predictions further, both these uncertainties need to be reduced. For the re-entry predictions of GOCE, this problem was partly negated by the the attitude control. However, for the Delta-K rocket stages and CHMAP the problem is present.

5 Critical assessment (WP410)

5.1 Research questions

The main technical objective of the study was to analyse the available measurements during the deorbit phase of the GOCE satellite, and to perform accompanying simulations, in order to provide answers to a number of research questions.

The following research questions were investigated:

RQ1 How well do trajectory and attitude predictions, made using only the data that would have been available at various epochs in the days and weeks before the actual re-entry, compare with the actual re-entry trajectory and attitude of GOCE?

RQ2 What were the main drivers of atmospheric variability along the GOCE trajectory in the final weeks, days and hours before its re-entry?

RQ3 How well were atmospheric models able to represent the atmospheric state at GOCEs locations?

RQ4 What information on the aerodynamic drag and lift accelerations on GOCE can be obtained from the GOCE data and to which extent can the models used in re-entry orbit determination and prediction correctly represent and/or predict these aerodynamic drag and lift accelerations?

RQ5 What is the influence on the re-entry prediction accuracy of the availability and accuracy of the observations typically used in such predictions, and which observation scenarios would lead to an optimal prediction accuracy?

RQ6 To which extent can the answers to the above questions, which were based on the analysis of GOCE data, be considered valid, or be extended to be valid, for the re- entry predictions of other space objects?

In WP110 precise orbit determination of GOCE and a detailed assessment of these results was performed. In WP210 actual and simulated TIRA observations were similarly assessed, as well as orbit solutions obtained from TLEs.

Due to additional tracking of JSpOC of GOCE during it's re-entry the TLE frequency nearly doubled. Also, two types of TLEs were found to be present for this period: a roughly equaly mix of enhanced and classic TLEs. The enhanced TLEs were found to have a reduced initial uncertainty of nearly half and improved (forward) propagation stability, compared to classic TLEs. As a result of this both types were considered separately for re-entry analysis.

As uncertainty information is not available for TLEs, a method was developed for estimating the initial covariance matrix using only TLE data. The results were compared against covariances obtained from GPS and gave mixed results. The initial uncertainty and strong correlations can be estimated reliably, while (weak to moderate) correlations prove more difficult. It was shown that these correlations were particularly sensitive.

In WP220 the modelling and simulation of GOCE's re-entry was considered. The resulting re-entry predictions were compared amongst each other and to the actual re-entry trajectory of GOCE.

First the effect of the modelling was investigated. Variations that were investigated include controlled and uncontrolled attitude, rigid body and point-mass attitude dynamics, biased and unbiased atmosphere, and a reduced atmospheric uncertainty.

Attitude control and atmospheric bias were found to have a significant effect on the prediction accuracy. The strong magnetorquers were able to maintain a stable attitude for a major part of the re-entry phase, while the atmospheric density was found to be significantly lower than predicted, both having a prolonging effect.

It was found that modelling of the attitude control was therefore crucial to providing realistic re-entry simulations for rigid body analysis in the case of GOCE. On the other hand, point-mass simulations provided a too optimistic attitude scenario, overshooting the true decay epoch.

The atmospheric density uncertainty was dominant in the prediction accuracy. It was demonstrated that if the atmospheric density uncertainty was halved, the decay-time uncertainty is reduced almost 40%.

The uncertainty outweighs all other contributions, such as the different initial uncertainties of the different state sets, which differed from decimetre level for GPS to kilometre level for TLEs. However, GPS obtained input for re-entry simulations was found most accurate, due to its better estimate of the density bias.

The re-entry simulations showed that scenarios, that consider higher availability of and more accurate observations, leading to better initial state accuracy will not directly reduce re-entry predictions uncertainty by a significant margin. The prediction precision was found to be driven mainly by the atmospheric density uncertainty in the current situation.

However, improved observation availability and accuracy, in the case of TIRA and TLEs, will lead to better estimates of the ballistic coefficient and therefore the atmospheric bias. This was shown to improve the prediction accuracy.

The increase TLE update frequency and presence of both (new) enhanced and (older) classic type of TLEs are indicating that JSpOC increased its tracking of GOCE during its re-entry phase. The (extra) classic TLEs were shown to be on average less accurate than the enhanced TLEs and have large fluctuations in their accuracy.

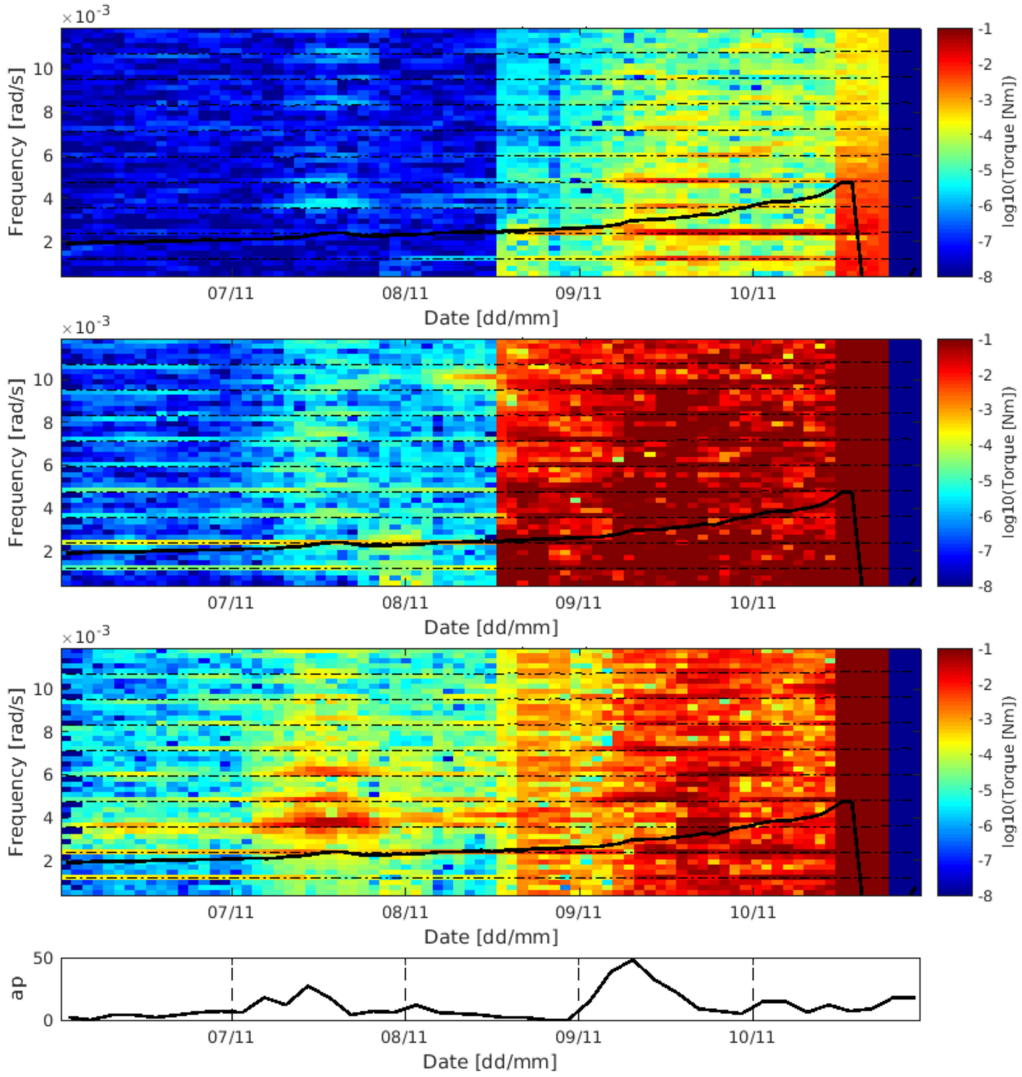

Figure 8: Power Spectral Density (colour) over frequency (vertical axis) and time (horizontal axis) of the measured torque derived from the measured angular acceleration and rate during the de-orbit phase in roll (top), pitch (middle) and yaw direction.

TLE simulated from high-precision GPS orbits, under idealised observation conditions, were shown to have accuracy comparable to the actual published TLEs. This illustrates that also for the TLEs, higher availability will not significantly improve the state estimation.

The fact that GOCE was under active attitude control limits somewhat the extension of results to other objects. However, it was found that the magnetic torquers acted mainly in the pitch and roll direction, and that the yaw motion was dominated by the aerodynamics.

5.1.1 Aerodynamic resonance

Inspired by the results by James Beck of Belstead Research Ltd., presented at the joint final presentation, a frequency analysis was made of the torques acting on GOCE in the de-orbit phase. The evolution of the Power Spectral Densities (PSDs) are plotted over time in figures 8 and 9 for the measured and aerodynamic torque respectively. Note that the measured angular acceleration saturates just after noon on November 8, when Accelerometer 3 gets stuck at the saturation level.

Most interesting is the trend observed in the yaw direction. The frequency with the largest response increases towards re-entry, following the trend of the modelled aerodynamic frequency (black line, provided by James Beck). Although many of the increases in intensity occur during increased geomagnetic activity, there is reason

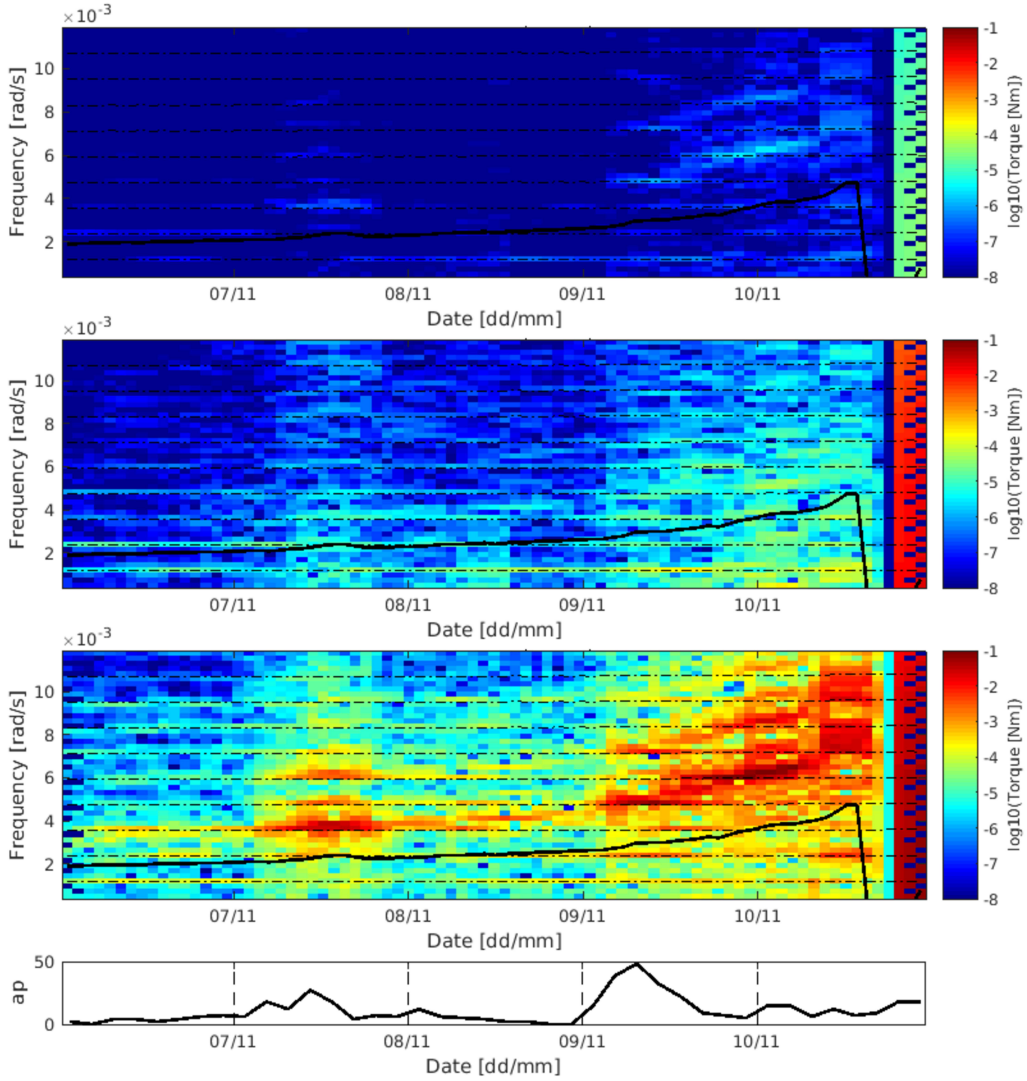

Figure 9: Power Spectral Density (colour) over frequency (vertical axis) and time (horizontal axis) of the modelled aerodynamic torque during the de-orbit phase in roll (top), pitch (middle) and yaw direction.

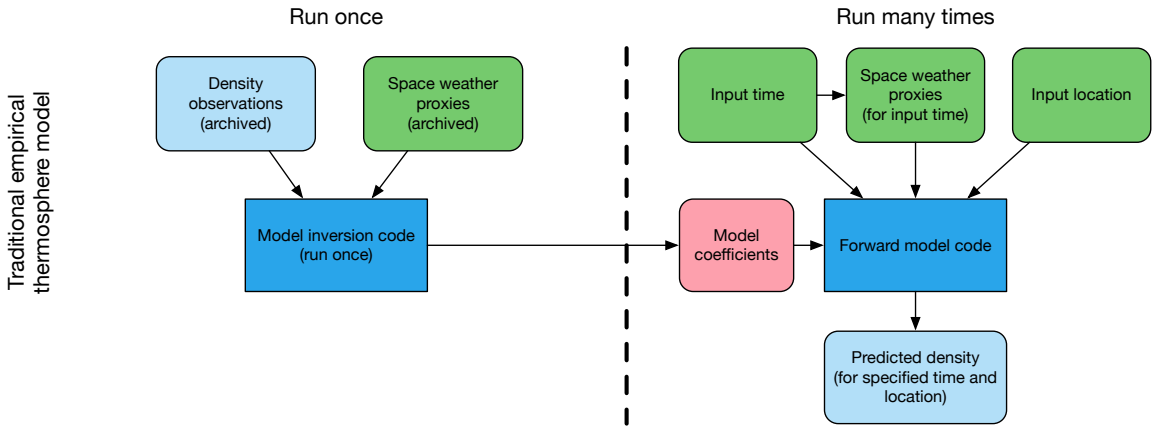

Figure 10: Flow chart for the generation and use of a traditional empirical model.

to believe that the aerodynamic frequency resonates with modes of the orbital frequency (dashed-dotted lines). This claim is supported by the fact that the maximum response peak lingers on the fourth and fifth orbital mode on November 9 and 10. As the aerodynamic torque is by far the largest in the yaw direction, it is expected that GOCE resonates with an aerodynamic signal such as winds or varying density.

The results also raise at least two more questions. First, it is interesting to analyse what would have happened had a strong geomagnetic storm hit during the re-entry. Would GOCE have responded stronger, or possibly even have started tumbling, despite its attitude control? Second, it is worth investigating whether this behaviour can be generalized to other aerodynamically stable debris objects. Would it be possible to predict these oscillations, and consequently refine our estimates of frontal area and drag? Combining the two questions, it may even be possible to improve the prediction of the level of geomagnetic activity at which a transition tumbling motion could occur for such debris objects. It is to be expected that this behaviour will be observed in other (passively) aerodynamically stable objects as they de-orbit.

5.2 Recommendations

The atmospheric density modelling and rotational motion modelling and estimation have been identified as the main contributors to the re-entry predictions uncertainty. To further improve re-entry predictions, the following recommendations for future research have been identified.

5.2.1 Improve Rotational Uncertainty Models and Estimation

High-fidelity re-entry simulations, involving rigid-body dynamics and propagation of multi-dimensional error distributions, provide accurate and reliable predictions. Such analysis is relatively easy to implement for groups of objects, such as rocket bodies, or high-interest objects. The quality of the predictions, however, depend on proper modelling of the (initial) uncertainties and accurate estimation of its parameters.

For many objects, TLEs present the only source of specific data available. The problem of the initial translational uncertainty was already addressed in this study. However, the initial rotational state is often completely unknown and hard to estimate. For the re-entry predictions of GOCE, this problem was partly negated by the modelling of the attitude control. Therefore, the influence of these contributions was not directly investigated. However, for uncontrolled spacecraft, as demonstrated for the Delta-K rocket stages and CHMAP the problem remains. Further research into improving these re-entry simulations should investigate methods that reduce uncertainties and/or correlate uncertainty components related to the rotational state.

5.2.2 Development of an updated near real-time thermosphere density model

The accuracy of the empirical thermosphere density model was found to have a dominant effect on re-entry prediction uncertainty. The current paradigm for such models, which include NRLMSISE-00, JB-2008 and

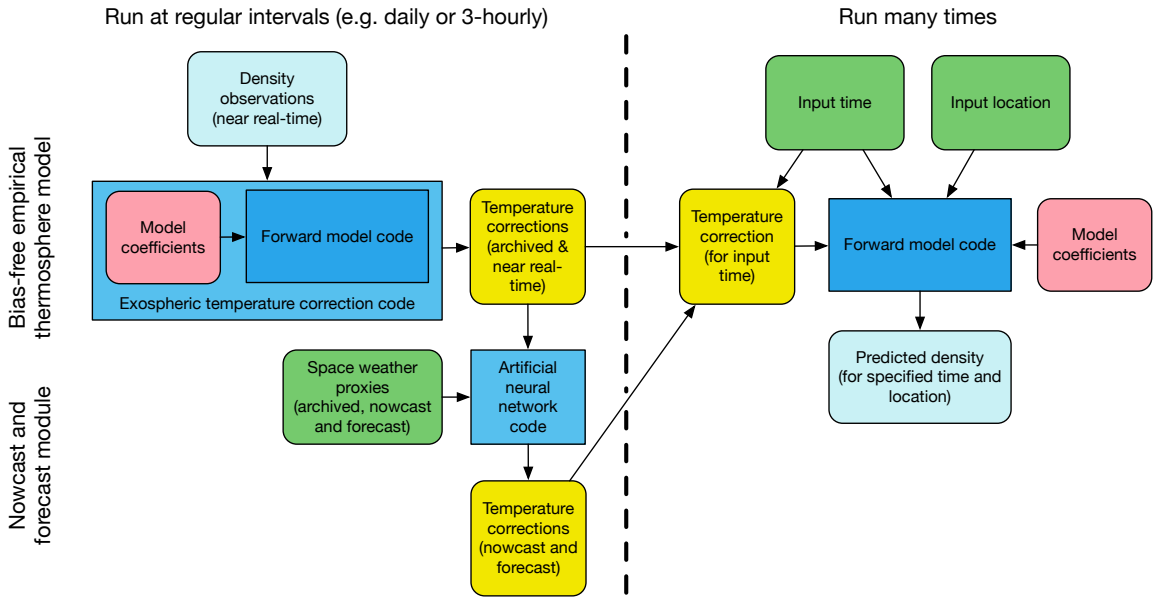

Figure 11: Flow chart for the use of an empirical thermosphere model with data assimilation and prediction capability.

DTM2013, shown as a flow-chart in Figure 10, is outdated. These models are currently completely based on past databases of density observations (and in some cases including temperature and composition data as well), combined with space weather proxies and indices for this observation period. These databases are used to generate a set of coefficients for the parametrised model, which is then driven by current proxies and indices. The density variability that is not captured by the parametric equations, as well as any errors in the proxy prediction, can cause large errors.

During orbit determination of space debris, the density model errors is usually absorbed in the ballistic coefficient estimate or drag scale factor. The large fluctuations of the density errors can sometimes make it difficult to identify changes in the frontal area of the object in the time series of estimated ballistic coefficients.

Figure 11 shows a modified flow-chart, for a next-generation thermosphere model. The flow-charts are taken from a joint EU proposal by Eelco Doornbos at TU Delft and Sean Bruinsma at CNES, and are partly based on earlier work on the NRTDM model developed by Doornbos under ESOC contract and the DTM-nrt model developed by Bruinsma as part of the EU FP7 ATMOP project. These models, both based on the US Air Force HASDM model, can be considered the prototype for the next generation model shown in the flow-chart.

The most important element in the next generation model is the capability to estimate temperature corrections at regular intervals (e.g. daily or 3-hourly). These corrections are estimated from near real-time density observations. In the NRTDM model, TLE data formed the input. However, the data had a very poor temporal resolution. The HASDM model is based on space surveillance tracking data, but this type of data is currently not sufficiently available in Europe for this purpose. The proposal for the next generation model therefore uses density data derived in near real-time from accelerometer data, or precise GNSS tracking of LEO Earth Observation satellites, such as the Earth Explorers, PROBA-2, PROBA-V and the Sentinels. If such data can be made available in near real-time, this would most likely allow for even greater precision than space surveillance tracking. The exospheric temperature correction, which could be based on a simple inversion, would ensure that the model output could be nearly free of bias.

A second important element of the next generation model is the prediction branch, shown at the bottom-left of Figure 11. This branch takes the near real-time and archived temperature corrections as input, together with archived, nowcast and forecast space weather proxies. This information is used in an artificial neural network algorithm, to provide a forecast of the temperature correction values.

Users of the model will now be able to run the forward model code using a predicted temperature correction as an input, replacing the (predicted) space weather proxy. The advantage is that the predicted temperature correction combines information on the current state of the atmosphere and its response to solar input, based on the near real-time density observations, as well as on the expected state of the solar input.

References

ESA (2015), Statement of Work, ESA Express Procurement "EXPRO", Benchmarking re-entry prediction uncertainties, GSP-REN-SOW-00138-HSO-GR, Issue 1, Revision 6, 26/03/2015.

Lemmens, S., B. Bastida Virgili, T. Flohrer, F. Gini, H. Krag, and C. Steiger (2015), Calibration of radar based re-entry predictions, in *Proceedings of the 5th International GOCE User Workshop, 25 - 28 November 2014, UNESCO, Paris,France*, number SP–728, pp. 2–9, ESA.

Liu, H.-L., B.T. Foster, M.E Hagan, and et al. (2010), Thermosphere extension of the Whole Atmosphere Community Climate Model, *J. Geophys. Res.*, *115*, A12302.

TU Delft, HTG, and BAS (2017), Benchmarking re-entry prediction uncertainties, *Final Report, ESA Contract No. 4000115171/15/F/MOS*, March 2017.